

DESI constraints on varying electron mass model and axion-like early dark energy

Osamu Seto^{*} and Yo Toda[†]

Department of Physics, Hokkaido University, Sapporo 060-0810, Japan

Abstract

Baryon acoustic oscillation (BAO) is one of the important standard ruler in cosmology. The results of the latest BAO measurements by Dark Energy Spectroscopic Instrument (DESI) survey has been reported. Cosmology with the varying electron mass model and the early dark energy (EDE) models are regraded as interesting models to resolve the Hubble tension. We present constraints on the varying electron mass model and EDE models by including new DESI data as well as cosmic microwave background by Planck and the conventional BAO data from 6dF, MGS, and DR12 and supernovae light curve data into analysis. Since new DESI BAO data indicates slightly longer sound horizon r_{dh} than the other BAO observations, for the varying electron mass model, the larger $H_0 = 69.44 \pm 0.84$ km/s/Mpc is indicated.

^{*} seto@particle.sci.hokudai.ac.jp

[†] y-toda@particle.sci.hokudai.ac.jp

I. INTRODUCTION

The Λ CDM model has been successful in explaining observations of the universe at various redshifts. However, as observations have become more precise, a discrepancy has emerged between the Hubble constants from distant (high redshifts) observations and local (low redshifts) observations. The spectrum of temperature anisotropy of the cosmic microwave background (CMB) infers the present Hubble parameter as $H_0 = 67.36 \pm 0.54 \text{ km/s/Mpc}$ [1]. By combining CMB, baryon acoustic oscillations (BAO) and Big Bang nucleosynthesis (BBN) data, we find $H_0 = 67.6 \pm 1.0 \text{ km/s/Mpc}$ [2]. Other distant observations [3–5] also report consistent values of H_0 with the Planck measurement. On the other hand, local measurements of the Hubble constant have reported as $H_0 = 73.04 \pm 1.04 \text{ km/s/Mpc}$ by the SH0ES [6] and $H_0 = 73.30^{+1.7}_{-1.8} \text{ km/s/Mpc}$ by the H0LiCOW [7]. The method of SNe Ia and the Tip of the Red Giant Branch (TRGB) observations reported a slightly lower Hubble constant, $H_0 = 69.6 \pm 2.5 \text{ km/s/Mpc}$ [8]. This discrepancy is called the Hubble tension.

Among various ideas to solve the Hubble tension [9–14], the varying electron mass (varying m_e) model and the early dark energy (EDE) models are regarded as the most promising solutions [13]. If we assume that the electron mass was larger by a few percent than the present value $m_{e0} = 511 \text{ keV}$ before the recombination epoch $z \gtrsim 1000$, then the varying electron mass model seems a potential solution to the Hubble tension [15–19], because shorter sound horizon scale at the recombination epoch indicates smaller H_0 .

The EDE model [20–28] has been intensively also studied as a possible solution to the H_0 tension. In the EDE model, temporal energy of EDE before the recombination epoch makes the sound horizon shorter, which results in smaller inferred H_0 . The EDE models are constrained not to increase the amplitude of matter fluctuation σ_8 [20] or the baryon density $\Omega_b h^2$ [29, 30].

Many models of EDE are proposed with different potentials, but in this paper, we focus on the axion-like EDE [20], which could explain the cosmic birefringence [31, 32] suggested by the recent analyses of the Planck data [33, 34].

Dark Energy Spectroscopic Instrument (DESI) survey has reported the results of the latest BAO measurements [35, 36] and that the cosmological constant dark energy (w, w_a) = $(-1, 0)$ is 2.1σ discrepant with the combination analysis of DESI+SDSS+CMB+PantheonPlus [37],

where w_a is the derivative of the equation of the parameter w with respect to the scale factor a . To explain this result, many extended models of dark energy have been discussed [38–47]. In this paper, we discuss implication of the DESI BAO results to the varying m_e model and the axion-like EDE model.

This paper is organized as follows. We present the explanation of the model in Sec II, the method and the data sets of our analysis in Sec. III, the results in Sec. IV, and the summary in Sec V.

II. MODELS

A. Varying electron mass

In the varying electron mass model, we assume that the value of the electron mass at early Universe differs from its present value and it dramatically changes to the current value after the recombination is complete. As discussed in the previous work [15], the primary contribution of an increased electron mass is the increasing energy level of hydrogen and Lyman alpha photon, both of which are directly proportional to the electron mass $E \propto m_e$. Since the energy level of hydrogen is higher, a photon energy at the standard recombination temperature is too small to excite the hydrogen. In theory with large electron mass, the recombination takes place earlier than the standard and the resultant sound horizon becomes shorter. Thus, to reproduce the same measured multiple moment of acoustic peaks of CMB power spectrum, the larger electron mass results in a shorter diameter distance and a higher H_0 .

Another consequence of the increased electron mass is Thomson scattering rate σ_T which is proportional to m_e^{-2} and suppresses the peak of high- l CMB power spectrum. The other minor contributions include the photoionization cross-sections, the recombination coefficient, K-factors, Einstein A coefficients, and the two-photon decay rates (see Ref. [15] for the detail).

The varying electron mass model can significantly relieve the Hubble tension without spoiling the CMB fitting because there is the degeneracy between cold dark matter density $\omega_c = \Omega_c h^2$, baryon density $\omega_b = \Omega_b h^2$, and the sound horizon scale in the CMB spectrum,

which transformed into the degeneracy between m_e and H_0 . On the other hand, the BAO bound can resolve this degeneracy, a negative Ω_K model with positive spatial curvature $K > 0$ weakens the BAO constraints on variation of m_e nevertheless. Therefore, it is also important to consider the combination of varying $m_e + \Omega_K$ [16].

To examine the varying electron mass model, we make all the above mentioned modifications to the recombination code `recfast` [48] and perform the MCMC analysis sampling $m_e \in [0.9, 1.2]$ in addition to the 6 standard parameters.

B. Axion-like EDE

The potential of the axion-like EDE takes the form [20]

$$V(\phi) = \Lambda^4 \left(1 - \cos \left(\frac{\phi}{f} \right) \right)^n, \quad (1)$$

where Λ is the energy scale of the potential, f is the breaking scale of shift symmetry, and n is the power index of the cosine function. As in the previous paper by Poulin et al [21], we use the three phenomenological parameters: z_c , Θ_i , and $f_{\text{de}}(z_c) \equiv \frac{\rho_{\text{de}}(z_c)}{\rho_{\text{tot}}(z_c)}$, which stand for the redshift when ϕ starts to oscillate, the initial value of the scalar field ϕ/f , and the energy fraction of EDE to the total energy density ρ_{tot} at z_c . After the transition $z < z_c$, the energy density of EDE decreases as $\rho_{\text{de}} \propto a^{-4}$ for $n = 2$, which is faster than the background energy density does.

To examine the axion-like EDE, we use the `camb` [49] where axion-like EDE is already implemented and perform the MCMC analysis sampling $f_{\text{de}}(z_c) \in [0.00001, 0.15]$, $z_c \in [1000, 50000]$, and $\Theta_i \equiv \phi_{\text{ini}}/f \in [0.01, 3.14]$ in addition to the 6 standard parameters.

III. DATA SETS AND METHODOLOGY

We perform a Markov-chain Monte Carlo (MCMC) analysis on the time-varying electron mass model and the axion-like EDE, using the public MCMC code `CosmoMC-planck2018` [50]. We analyze the models by referring to the following cosmological observation and we call the above three data \mathcal{D} that are always included.

- CMB from Planck [1]. We use the temperature and polarization likelihoods for high l

plik ($l = 30$ to 2508 in TT and $l = 30$ to 1997 in EE and TE) and lowl Commander and lowE SimAll ($l = 2$ to 29). We also include CMB lensing [51].

- BAO from 6dF [52], MGS [53], and DR12 [54].
- light curve of SNeIa from *Pantheon* [55].
- DESI BAO [37].

IV. RESULTS

We present the results of models we have examined. Those likelihood are shown in Fig. 1 and parameter values in the best-fit points are listed in Tab. I.

We find that the DESI BAO results disfavor lower m_e and indicate slightly larger electron mass $m_e/m_{e0} = 1.0092 \pm 0.0055$ (CMB+BAO+DESI BAO). This indicates the shorter sound horizon at the recombination and larger H_0 than the analysis without DESI BAO. This is due to the measured sound horizon r_d relative to the diameter distance r_d/D by DESI BAO. Here, we define the sound horizon

$$r_d = \int_{z_d}^{\infty} \frac{c_s(z)}{H(z)} dz, \quad (2)$$

$$D_M = \frac{c}{H_0 \sqrt{\Omega_K}} \sinh \left[\sqrt{\Omega_K} \int_0^z \frac{dz'}{H(z')/H_0} \right], \quad (3)$$

$$D_H = \frac{c}{H(z)}, \quad (4)$$

and $D_V = (z D_M(z)^2 D_H(z))^{1/3}$, where z_d is the redshift of the drag epoch. Diameter distance D is inversely proportional to the Hubble constant H_0 . Therefore, in the BAO measurements, a product of the sound horizon and the Hubble constant $r_d h$ is constrained. For the greater electron mass, the Hubble constant H_0 increases while the sound horizon r_d slightly decreases, and the product $r_d h$ increases, which is preferred from DESI BAO measurements as in Fig. 1.

We show the best-fit point of $(\Omega_m, r_d h) = (0.3094, 99.773 \text{ km/s})$ for $m_e/m_{e0} = 0.99$ and $(\Omega_m, r_d h) = (0.2979, 101.364 \text{ km/s})$ for $m_e/m_{e0} = 1.01$ for the data combination of CMB+BAO+JLA+DESI BAO, in the Tab II. As a result using only DESI BAO analysis, we quote $(\Omega_m, r_d h) = (0.295, 101.8 \text{ km/s})$ for the best-fit point of Λ CDM model from the DESI paper [37]. By comparing those, for the smaller electron mass, the Hubble constant

H_0 becomes too small, and the sound horizon relative to the diameter distance $r_d/D \propto r_d h$ becomes too short, which leads to poor DESI fitting. The difference in the χ^2 values accounts for $\Delta\chi^2_{\text{DESI, bestfit}(m_e/m_{e0}=0.99)} - \Delta\chi^2_{\text{DESI, bestfit}(m_e/m_{e0}=1.01)} \simeq 4.7$ as in Tab II. Figs. 2, 3, and 4 show the comoving diameter distance over the sound horizon at the drag epoch $D_M/r_d(z)$, the Hubble distance over the sound horizon at the drag epoch $D_H/r_d(z)$ and the angle-average distance over the sound horizon at the drag epoch $D_V/r_d(z)$ of $m_e/m_{e0} = 1.01$ and 0.99 models, respectively, as the function of redshifts with the error bar of the DESI measurements.

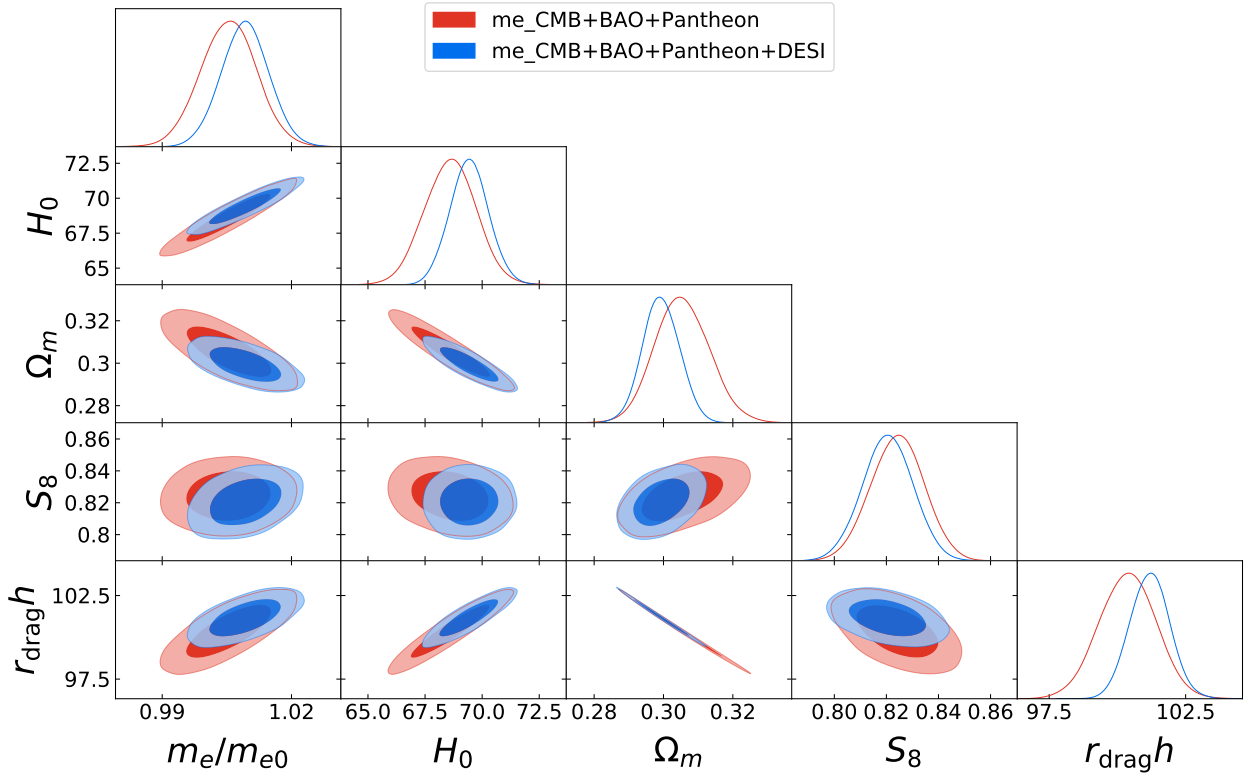


Figure 1: Posterior distributions of some parameters for the varying m_e model. Different colors of reddish and bluish contours stand for different data sets.

Next, we discuss the results of varying m_e in a curved Universe (the $m_e + \Omega_K$ model). As is shown in the DESI paper [37], we also find that a positive curvature ($K > 0$) model does not fit the DESI BAO data and a spatially flat ($K = 0$) Universe is preferred when DESI BAO data are included. The central value of a Hubble constant shifts slightly when DESI BAO data are incorporated. The results are summarized in Fig. 5 and Tab. I.

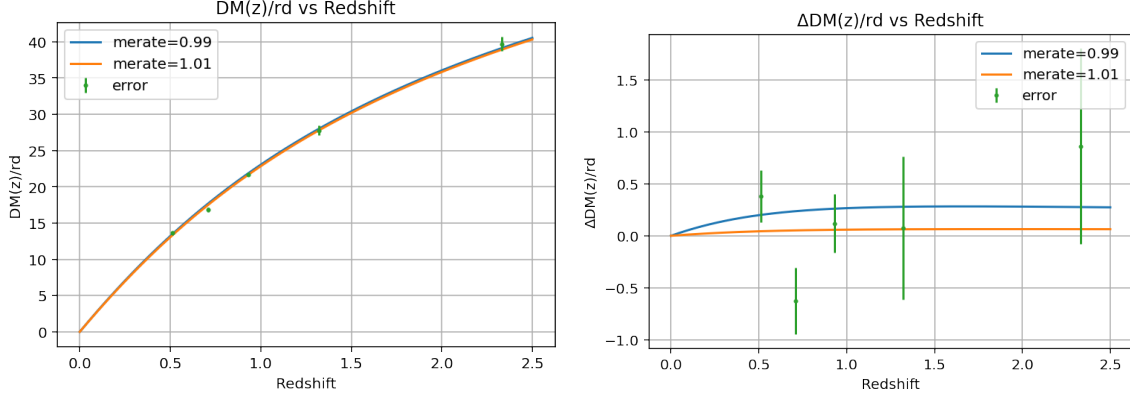


Figure 2: The comoving diameter distance over the sound horizon at the drag epoch $D_M/r_d(z)$ as a function of redshift. We use the best-fit value at $m_e = 1.01$ for the orange curve and $m_e = 0.99$ for the blue curve. The green error bars represent the data from the DESI BAO measurements. In the right panel, we illustrate the difference from the $D_M(z)/r_d$ assuming $(\Omega_M, r_{dh}) = (0.295, 101.8)$ which is the mean value from the only DESI BAO constraint [37].

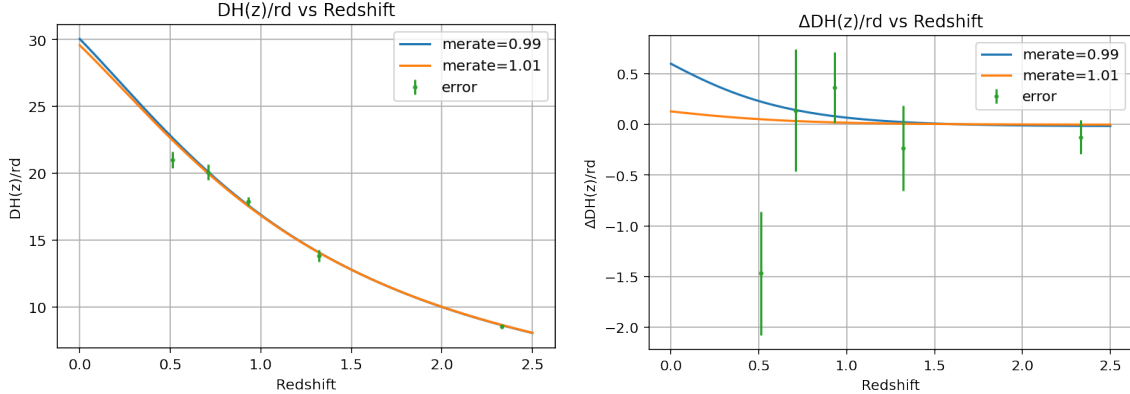


Figure 3: Same as Fig. 2, for the Hubble distance over the sound horizon at the drag epoch $D_H/r_d(z)$ as a function of redshift.

We present the results of axion-like early dark energy, which is given in Fig. 6 and Tab. I. As in the varying m_e model, we find a higher Hubble constant and a lower Ω_m when DESI BAO data are included. This result is in agreement with the previous paper [44], while authors of Ref. [44] have considered the $n = 3$ model and excluded other BAO data.

Finally, we calculate the Gaussian tension in Tab. I to make a fair comparison of the

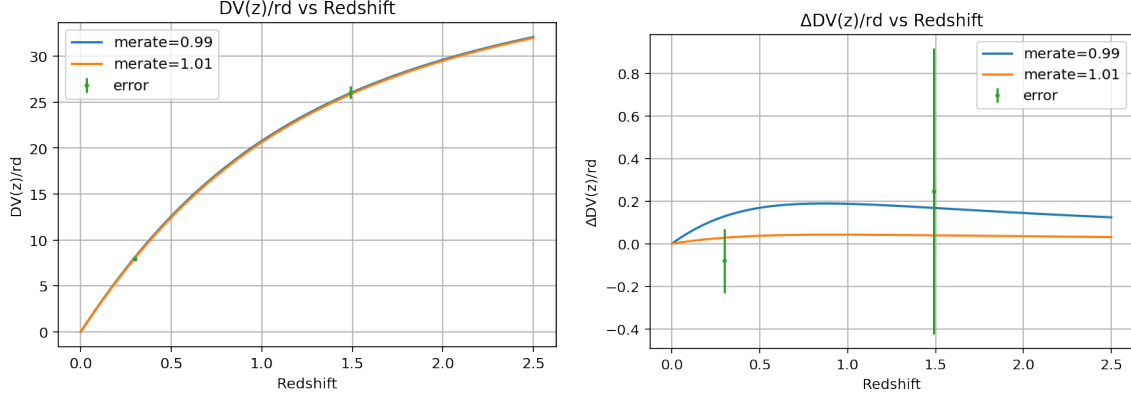


Figure 4: Same as Fig. 2, for the angle-average distance over the sound horizon at the drag epoch $D_V/r_d(z)$ as a function of redshift.

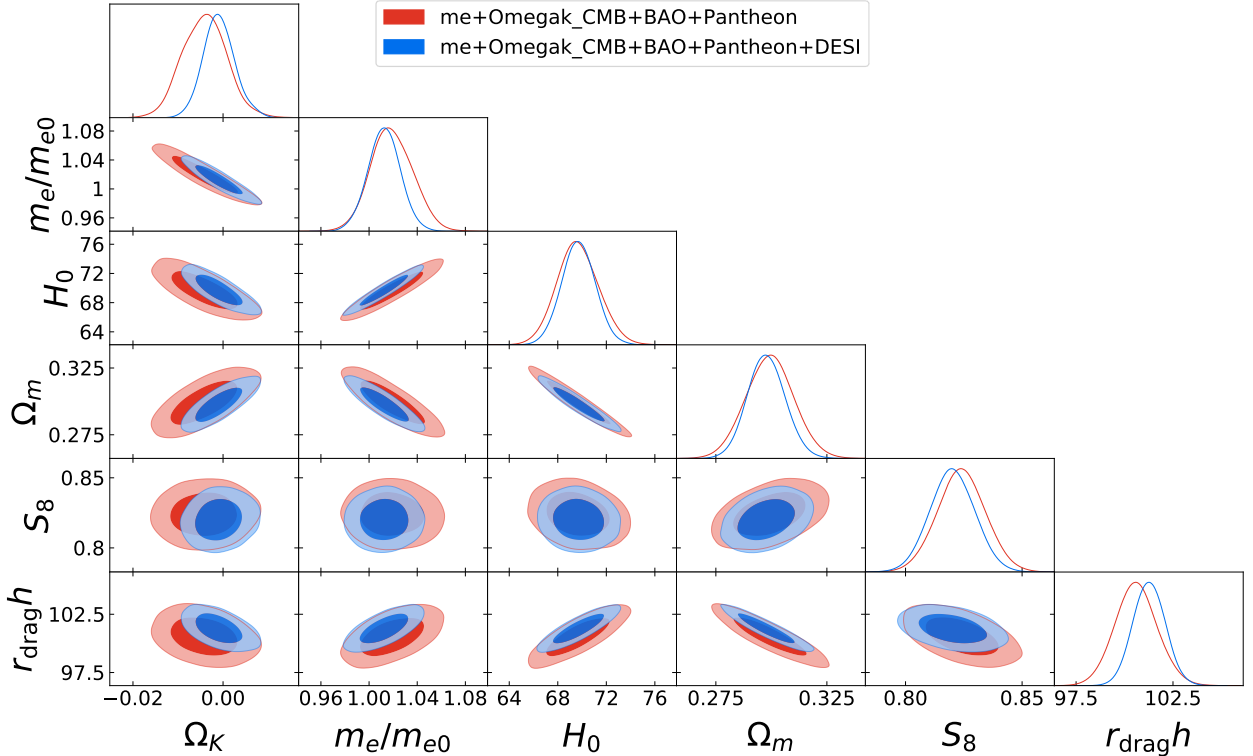


Figure 5: Posterior distributions of some parameters for the $m_e + \Omega_K$ model. Different colors of reddish and bluish contours stand for different data sets.

three models. The Gaussian tensions for H_0 , S_8 , and $\Omega_b h^2$ are respectively calculated as

$$T_{H_0} = \frac{H_0|_{\mathcal{D}(\text{w./w.o. DESI})} - 73.30}{\sqrt{\sigma_{\mathcal{D}(\text{w./w.o. DESI})}^2 + 1.04^2}}, \quad (5)$$

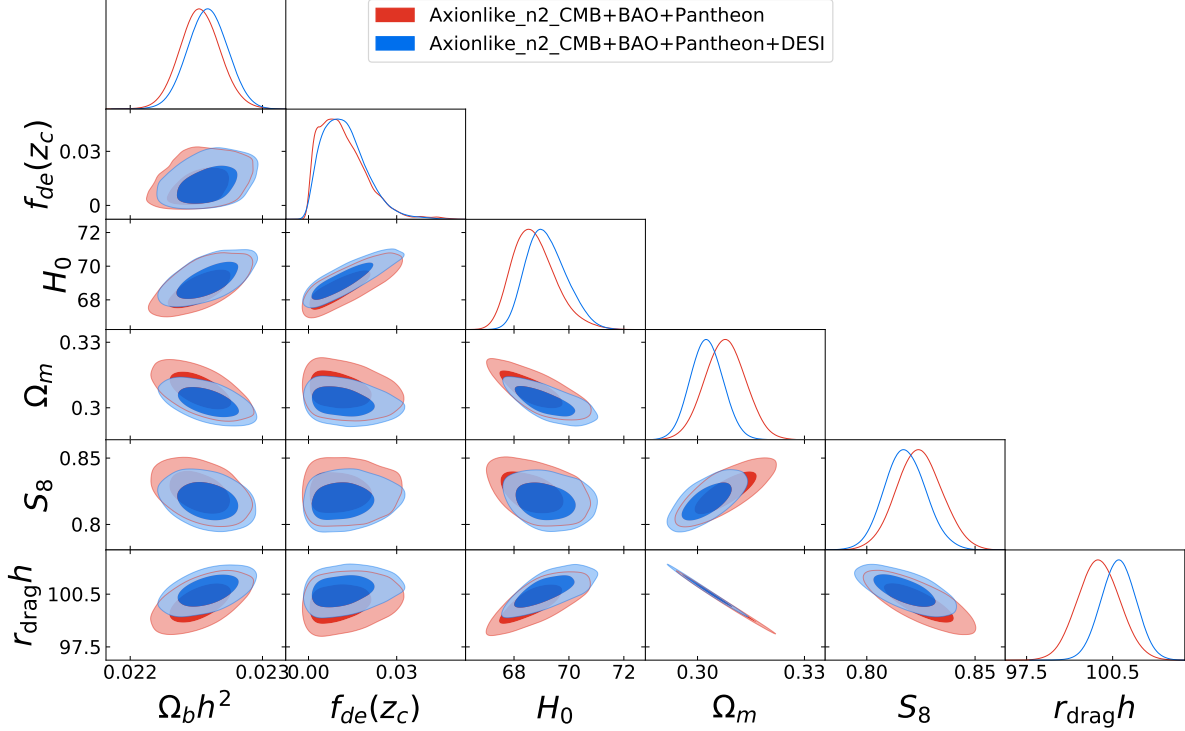


Figure 6: Posterior distributions of some parameters for axion-like EDE ($n = 2$) model.

Different colors of reddish and bluish contours stand for different data sets.

for the Hubble tension with direct measurement [6],

$$T_{S_8} = \frac{S_8|_{\mathcal{D}(\text{w./w.o. DESI})} - 0.776}{\sqrt{\sigma_{\mathcal{D}(\text{w./w.o. DESI})}^2 + 0.017^2}}, \quad (6)$$

for the S_8 tension with DES [56].

From the viewpoint of the Hubble tension, as in Tab. I, including DESI BAO data improves the tension in varying m_e model and the EDE models because DESI BAO indicate slightly shorter r_d . On the other hand, the tension increases for the varying $m_e + \Omega_K$ model, because the center value does not change but the error is reduced by breaking the degeneracy. In the respect of the S_8 tension, including DESI BAO data improves the tension in all three models.

V. CONCLUSIONS

In this paper, we examine the varying electron mass model and the axion-like early dark energy model, considering the recent DESI BAO measurements. In the analysis using a

combination of CMB, conventional BAO and light curves (Pantheon), as in the previous studies, we find that the electron mass before the CMB era is in agreement with the current value in a 1σ confidence level. However, when the DESI BAO data is included, we find that the larger electron mass is preferred as,

$$\left\{ \begin{array}{l} m_e/m_{e0} = 1.0054 \pm 0.0065 \\ H_0 = 68.6 \pm 1.1 \text{ km/s/Mpc} \quad (\text{CMB + BAO + Pantheon}), \\ \Omega_m = 0.3054 \pm 0.0078 \end{array} \right. \quad (7)$$

$$\left\{ \begin{array}{l} m_e/m_{e0} = 1.0092 \pm 0.0055 \\ H_0 = 69.44 \pm 0.84 \text{ km/s/Mpc} \quad (\text{CMB + BAO + Pantheon + DESI BAO}). \\ \Omega_m = 0.2993 \pm 0.0053 \end{array} \right. \quad (8)$$

Although the electron mass in the BAO era is assumed to be the same as today, the larger electron mass at CMB era leads to a higher Hubble constant H_0 and a product of a sound horizon and Hubble constant $r_d h$ to fit the CMB power spectrum, bringing it closer to the DESI best-fit value. This is the reason why DESI BAO data prefers the larger electron mass in the CMB era. It is also known that both m_e/m_{e0} and H_0 increase when considering a closed universe, but we find that such the case is not preferred from DESI BAO measurements.

In the axion-like EDE ($n = 2$) model, we also find that a larger amount of the EDE and a higher Hubble constant are preferred when the DESI BAO data is included.

ACKNOWLEDGMENTS

This work was supported by JSPS KAKENHI Grant Number 23K03402 (OS), and JST SPRING, Grant Number JPMJSP2119 (YT).

[1] N. Aghanim et al. (Planck), *Astron. Astrophys.* **641**, A6 (2020), [Erratum: *Astron.Astrophys.* 652, C4 (2021)], [arXiv:1807.06209 \[astro-ph.CO\]](https://arxiv.org/abs/1807.06209).

- [2] N. Schöneberg, L. Verde, H. Gil-Marín, and S. Brieden, *JCAP* **11**, 039 (2022), arXiv:2209.14330 [astro-ph.CO].
- [3] D. Dutcher *et al.* (SPT-3G), *Phys. Rev. D* **104**, 022003 (2021), arXiv:2101.01684 [astro-ph.CO].
- [4] S. Aiola *et al.* (ACT), *JCAP* **12**, 047 (2020), arXiv:2007.07288 [astro-ph.CO].
- [5] N. Schöneberg, J. Lesgourgues, and D. C. Hooper, *JCAP* **10**, 029 (2019), arXiv:1907.11594 [astro-ph.CO].
- [6] A. G. Riess *et al.*, *Astrophys. J. Lett.* **934**, L7 (2022), arXiv:2112.04510 [astro-ph.CO].
- [7] K. C. Wong *et al.*, *Mon. Not. Roy. Astron. Soc.* **498**, 1420 (2020), arXiv:1907.04869 [astro-ph.CO].
- [8] W. L. Freedman, B. F. Madore, T. Hoyt, I. S. Jang, R. Beaton, M. G. Lee, A. Monson, J. Neeley, and J. Rich, (2020), 10.3847/1538-4357/ab7339, arXiv:2002.01550 [astro-ph.GA].
- [9] E. Di Valentino, O. Mena, S. Pan, L. Visinelli, W. Yang, A. Melchiorri, D. F. Mota, A. G. Riess, and J. Silk, *Class. Quant. Grav.* **38**, 153001 (2021), arXiv:2103.01183 [astro-ph.CO].
- [10] E. Abdalla *et al.*, *JHEAp* **34**, 49 (2022), arXiv:2203.06142 [astro-ph.CO].
- [11] L. Perivolaropoulos and F. Skara, *New Astron. Rev.* **95**, 101659 (2022), arXiv:2105.05208 [astro-ph.CO].
- [12] W. L. Freedman, *Astrophys. J.* **919**, 16 (2021), arXiv:2106.15656 [astro-ph.CO].
- [13] N. Schöneberg, G. Franco Abellán, A. Pérez Sánchez, S. J. Witte, V. Poulin, and J. Lesgourgues, *Phys. Rept.* **984**, 1 (2022), arXiv:2107.10291 [astro-ph.CO].
- [14] S. Vagnozzi, *Universe* **9**, 393 (2023), arXiv:2308.16628 [astro-ph.CO].
- [15] P. A. R. Ade *et al.* (Planck), *Astron. Astrophys.* **580**, A22 (2015), arXiv:1406.7482 [astro-ph.CO].
- [16] T. Sekiguchi and T. Takahashi, *Phys. Rev. D* **103**, 083507 (2021), arXiv:2007.03381 [astro-ph.CO].
- [17] O. Seto and Y. Toda, *Phys. Rev. D* **107**, 083512 (2023), arXiv:2206.13209 [astro-ph.CO].
- [18] K. Hoshiya and Y. Toda, *Phys. Rev. D* **107**, 043505 (2023), arXiv:2202.07714 [astro-ph.CO].
- [19] R. Solomon, G. Agarwal, and D. Stojkovic, *Phys. Rev. D* **105**, 103536 (2022), arXiv:2201.03127 [hep-ph].
- [20] V. Poulin, T. L. Smith, D. Grin, T. Karwal, and M. Kamionkowski, *Phys. Rev. D* **98**, 083525 (2018), arXiv:1806.10608 [astro-ph.CO].

- [21] V. Poulin, T. L. Smith, T. Karwal, and M. Kamionkowski, *Phys. Rev. Lett.* **122**, 221301 (2019), arXiv:1811.04083 [astro-ph.CO].
- [22] M. Braglia, W. T. Emond, F. Finelli, A. E. Gumrukcuoglu, and K. Koyama, *Phys. Rev. D* **102**, 083513 (2020), arXiv:2005.14053 [astro-ph.CO].
- [23] P. Agrawal, F.-Y. Cyr-Racine, D. Pinner, and L. Randall, *Phys. Dark Univ.* **42**, 101347 (2023), arXiv:1904.01016 [astro-ph.CO].
- [24] G. Ye and Y.-S. Piao, *Phys. Rev. D* **101**, 083507 (2020), arXiv:2001.02451 [astro-ph.CO].
- [25] T. L. Smith, V. Poulin, and M. A. Amin, *Phys. Rev. D* **101**, 063523 (2020), arXiv:1908.06995 [astro-ph.CO].
- [26] M.-X. Lin, G. Benevento, W. Hu, and M. Raveri, *Phys. Rev. D* **100**, 063542 (2019), arXiv:1905.12618 [astro-ph.CO].
- [27] F. Niedermann and M. S. Sloth, *Phys. Rev. D* **103**, L041303 (2021), arXiv:1910.10739 [astro-ph.CO].
- [28] F. Niedermann and M. S. Sloth, *Phys. Rev. D* **102**, 063527 (2020), arXiv:2006.06686 [astro-ph.CO].
- [29] O. Seto and Y. Toda, *Phys. Rev. D* **103**, 123501 (2021), arXiv:2101.03740 [astro-ph.CO].
- [30] T. Takahashi and Y. Toda, *JCAP* **11**, 101 (2023), arXiv:2306.00454 [astro-ph.CO].
- [31] L. M. Capparelli, R. R. Caldwell, and A. Melchiorri, *Phys. Rev. D* **101**, 123529 (2020), arXiv:1909.04621 [astro-ph.CO].
- [32] K. Murai, F. Naokawa, T. Namikawa, and E. Komatsu, *Phys. Rev. D* **107**, L041302 (2023), arXiv:2209.07804 [astro-ph.CO].
- [33] Y. Minami and E. Komatsu, *Phys. Rev. Lett.* **125**, 221301 (2020), arXiv:2011.11254 [astro-ph.CO].
- [34] P. Diego-Palazuelos et al., *Phys. Rev. Lett.* **128**, 091302 (2022), arXiv:2201.07682 [astro-ph.CO].
- [35] A. G. Adame et al. (DESI), (2024), arXiv:2404.03000 [astro-ph.CO].
- [36] A. G. Adame et al. (DESI), (2024), arXiv:2404.03001 [astro-ph.CO].
- [37] A. G. Adame et al. (DESI), (2024), arXiv:2404.03002 [astro-ph.CO].
- [38] Y. Tada and T. Terada, (2024), arXiv:2404.05722 [astro-ph.CO].
- [39] M. Cortês and A. R. Liddle, (2024), arXiv:2404.08056 [astro-ph.CO].

- [40] Y. Carloni, O. Luongo, and M. Muccino, (2024), arXiv:2404.12068 [astro-ph.CO].
- [41] W. Giarè, M. A. Sabogal, R. C. Nunes, and E. Di Valentino, (2024), arXiv:2404.15232 [astro-ph.CO].
- [42] O. Christiansen, F. Hassani, and D. F. Mota, (2024), arXiv:2405.00668 [astro-ph.CO].
- [43] H. Wang and Y.-S. Piao, (2024), arXiv:2404.18579 [astro-ph.CO].
- [44] F. J. Qu, K. M. Surrao, B. Bolliet, J. C. Hill, B. D. Sherwin, and H. T. Jense, (2024), arXiv:2404.16805 [astro-ph.CO].
- [45] G. Poulot, E. M. Teixeira, C. van de Bruck, and N. J. Nunes, (2024), arXiv:2404.10524 [astro-ph.CO].
- [46] D. Andriot, S. Parameswaran, D. Tsimpis, T. Wräse, and I. Zavala, (2024), arXiv:2405.09323 [hep-th].
- [47] M. C. Pookkillath and K. Koyama, (2024), arXiv:2405.06565 [gr-qc].
- [48] D. Scott and A. Moss, Mon. Not. Roy. Astron. Soc. **397**, 445 (2009), arXiv:0902.3438 [astro-ph.CO].
- [49] C. Howlett, A. Lewis, A. Hall, and A. Challinor, JCAP **04**, 027 (2012), arXiv:1201.3654 [astro-ph.CO].
- [50] A. Lewis and S. Bridle, Phys. Rev. D **66**, 103511 (2002), arXiv:astro-ph/0205436.
- [51] N. Aghanim et al. (Planck), Astron. Astrophys. **641**, A8 (2020), arXiv:1807.06210 [astro-ph.CO].
- [52] F. Beutler, C. Blake, M. Colless, D. Jones, L. Staveley-Smith, L. Campbell, Q. Parker, W. Saunders, and F. Watson, Mon. Not. Roy. Astron. Soc. **416**, 3017 (2011), arXiv:1106.3366 [astro-ph.CO].
- [53] A. J. Ross, L. Samushia, C. Howlett, W. J. Percival, A. Burden, and M. Manera, Mon. Not. Roy. Astron. Soc. **449**, 835 (2015), arXiv:1409.3242 [astro-ph.CO].
- [54] S. Alam et al. (BOSS), Mon. Not. Roy. Astron. Soc. **470**, 2617 (2017), arXiv:1607.03155 [astro-ph.CO].
- [55] D. M. Scolnic et al. (Pan-STARRS1), Astrophys. J. **859**, 101 (2018), arXiv:1710.00845 [astro-ph.CO].
- [56] T. M. C. Abbott et al. (DES), Phys. Rev. D **105**, 023520 (2022), arXiv:2105.13549 [astro-ph.CO].

Parameter	m_e	$m_e + \Omega_K$	EDE
$\Omega_b h^2$	0.02251 ± 0.00016	$0.02288^{+0.00045}_{-0.00050}$	0.02253 ± 0.00016
$\Omega_c h^2$	0.1205 ± 0.0019	0.1216 ± 0.0022	$0.1222^{+0.0016}_{-0.0026}$
m_e/m_{e0}	1.0054 ± 0.0065	1.019 ± 0.018	-
Ω_K	-	-0.0041 ± 0.0049	-
$f_{de}(z_c)$	-	-	$0.0117^{+0.0039}_{-0.010}$
H_0	68.6 ± 1.1	69.7 ± 1.7	$68.74^{+0.62}_{-0.90}$
Ω_m	0.3054 ± 0.0078	0.299 ± 0.011	0.3078 ± 0.0057
S_8	0.824 ± 0.010	0.824 ± 0.010	0.824 ± 0.011
T_{H_0}	3.10σ	1.81σ	3.51σ
T_{s_8}	2.43σ	2.43σ	2.37σ

Parameter	m_e	$m_e + \Omega_K$	EDE
$\Omega_b h^2$	0.02260 ± 0.00014	0.02269 ± 0.00036	0.02259 ± 0.00015
$\Omega_c h^2$	0.1210 ± 0.0018	0.1213 ± 0.0021	$0.1216^{+0.0016}_{-0.0026}$
m_e/m_{e0}	1.0092 ± 0.0055	1.013 ± 0.014	-
Ω_K	-	$-0.0009^{+0.0032}_{-0.0036}$	-
$f_{de}(z_c)$	-	-	$0.0123^{+0.0049}_{-0.0092}$
H_0	69.44 ± 0.84	69.7 ± 1.4	$69.19^{+0.60}_{-0.84}$
Ω_m	0.2993 ± 0.0053	0.2978 ± 0.0085	0.3026 ± 0.0046
S_8	0.8205 ± 0.0097	0.8201 ± 0.0096	0.8178 ± 0.0096
T_{H_0}	2.89σ	2.06σ	3.23σ
T_{s_8}	2.27σ	2.26σ	2.14σ

Table I: 68% constraints and Gaussian tension to other measurements from the data set \mathcal{D} (upper) and $\mathcal{D}+$ DESI (lower)

Parameter	$m_e=0.99$	$m_e=1.00$	$m_e=1.01$
Ω_m	0.3094	0.3045	0.2979
$r_d h$	99.773	100.448	101.364
χ^2_{CMB}	2782.28	2775.04	2774.53
χ^2_{6DF}	0.022	0.000	0.033
χ^2_{MGS}	1.279	1.677	2.271
χ^2_{DR12}	4.281	3.520	3.509
χ^2_{DESI}	17.739	15.051	13.060
χ^2_{JLA}	1034.959	1034.799	1034.736
χ^2_{prior}	2.059	2.052	1.874
χ^2_{Total}	3842.63	3832.14	3830.01

Table II: Best-fit point using \mathcal{D} + DESI